

HIGH ENERGY PHYSICS

Measuring the Cosmic-Ray Muon Decoherence Curve through Plastic Scintillators

Guilherme H. Caumo (260964615)

McGill University Department of Physics

November 1, 2024

Abstract

This study used a setup of plastic scintillation detectors and nuclear instrumentation (NIM) modules to measure the decoherence curve of cosmic-ray muons at sea level. The decoherence curve was calculated by measuring coincident muons over multiple detector separations in a given period. Thereafter, the data were analyzed by plotting the rates of muon coincidence with respect to the separations using a Nishimura-Kamata-Greisen (NKG) fit. Based on this, it was observed that the NKG fit adequately modeled the measured decoherence curve for cosmic-ray muons. In sum, this study successfully measured the decoherence curve of cosmic-ray muons, though future experiments should aim to achieve greater experimental accuracy and expand upon methods presented here to explore more properties of elementary particles.

1 Introduction

1.1 Theory

The muon was discovered in 1937 by C. W. Anderson and S. H. Neddermeyer by exposing a cloud chamber to cosmic-rays, marking a breakthrough in particle physics [1]. Cosmic-ray muons, μ^- and μ^+ , are created in the upper atmosphere when high-energy cosmic-ray particles, called primary particles, interact with the nuclei of atmospheric particles, a process that produces pions, π^+ and π^- , which in turn produce muons via their decays [2], such that:

$$\begin{aligned}\pi^+ &\longrightarrow \mu^+ + \nu \\ \pi^- &\longrightarrow \mu^- + \bar{\nu},\end{aligned}\tag{1}$$

where ν represents a neutrino and $\bar{\nu}$ an anti-neutrino. However, a charged pion has a long enough lifetime long to interact with an atmospheric particle's nucleus before it decays, creating a second generation of charged and neutral pions similar to the initial interaction; this process, therefore, creates cascades of particles called cosmic-ray air showers [3]. Because primaries come with velocities near that of light and very high energies, the products of air showers tend to move in the same direction as the primaries while spreading out from the central and vertical axis with every generation [3] [4].

Muons are highly penetrative particles born in air showers in the upper atmosphere that survive long enough to reach sea level [5]. Muons, like electrons, interact via weak and electromagnetic (EM) forces and, consequently, have less chance of being absorbed than pions [5] [6]. In addition, muons are less susceptible to losing energy due to EM radiation processes than electrons by having a mass 207 times greater [5] [7].

Since muons live long enough to reach the ground, these particles are fundamental in the study of air showers. More specifically, the lateral size of air showers can be characterized by measuring the decoherence curve for cosmic-ray muons. The decoherence curve for cosmic-ray muons is defined as the rate of muon coincidences in two detectors as a function of detector separations. Consequently, the muon decoherence curve is effectively modeled by the NKG

function, a well-established mathematical equation used to describe the lateral distribution of charged particles, such as muons [8]. The NKG function is such that, [9] [10]:

$$f(r) = c(s) \left(\frac{r}{r_m} \right)^{s-2} \left(1 + \frac{r}{r_m} \right)^{s-4.5}, \quad (2)$$

where, $f(r)$ is the particle density at distance r , r_m is the Molière radius describing the lateral size, s is the age parameter describing the broadening of the shower, and $c(s)$ is the normalization constant where,

$$c(s) = \frac{\Gamma(4.5 - s)}{2\pi r_m^2 \Gamma(s) \Gamma(4.5 - 2s)}. \quad (3)$$

Therefore, the NKG function can be fitted to the decoherence curve to extract the lateral size, age parameter, and normalization constant respective to the air-shower.

1.2 Experimental Goals

Considering the points above, this study aims to use a setup of photomultiplier tubes (PMTs) attached to plastic scintillators to measure the decoherence curve of cosmic-ray muons to help learn about techniques in experimental particle physics.

2 Methodology

2.1 Equipment and Calibration

This study's experimental design featured four plastic scintillation detectors, labeled A, B, C, and D, each composed of a PMT glued to a slab of plastic scintillator, and NIM modules, specifically a discriminator unit, a logic unit, and a counter.

Plastic scintillators are well-established in experimental setups involving charged particles [11]. Firstly, the scintillators of detectors A and B (28.4 cm x 10.5 cm x 2.83 cm) were wrapped in Tyvek reflective material and then wrapped further in black tape to prevent light leaks and external light sources from affecting the measurements. Next, the scintillators of detectors C and D (71 cm x 65 cm x 4.5 cm) were wrapped in Tyvek reflective material, wrapped

further with a black cloth, and then enclosed in a wooden box to prevent light leaks and provide mechanical structure, as shown in Figure 1. The PMTs were then attached to the scintillators using optical glue. Each PMT used in this study has a Cockcroft-Walton (CW) voltage multiplier attached to its base, which provides the necessary high voltage needed for the PMT to function. It multiplies its input voltage by a factor of 100 while also providing the output signal. Lastly, the output signal of each detector was recorded by an SDS1204X-E SIGLENT oscilloscope attached to a laptop running a Python program.

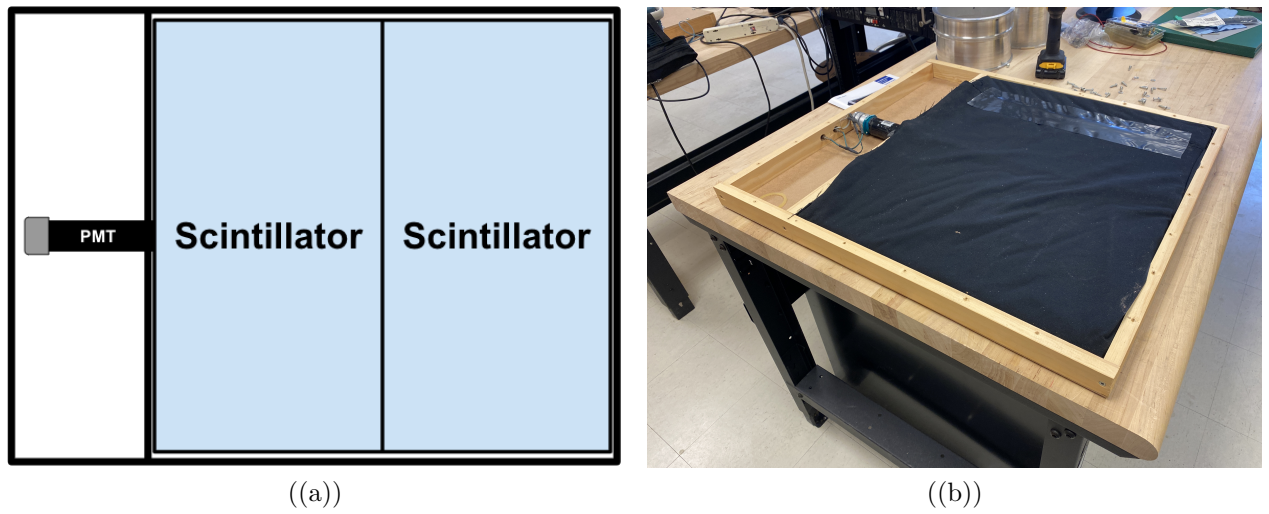


Figure 1: Structure of scintillation detectors C and D demonstrating plastic scintillators along with attached PMT and CW voltage multiplier. a) Diagram of the apparatus. b) Image of the apparatus with its top layer removed.

The calibration for the setup consisted of stacking detectors A, B, C, and D, as shown in Figure 2, so detectors A and B act as triggers while detectors C and D record muon traces at six different voltages (15 V, 16 V, 17 V, 18 V, 19 V, and 20 V). The recorded traces were then integrated to obtain the distribution of charges for the tested voltages, illustrated by the sample trace in Figure 3. In more detail, the charges were calculated by considering that the traces' voltages were divided by the 50Ω input impedance of a terminator placed at the oscilloscope's channel input. Hence, the voltages were converted into currents, i , in millamps, and these values were used to calculate the trace charges, Q , in picocoulombs due to the following relation:

$$Q = \int idt, \quad (4)$$

where dt represents the period of time being integrated in nanoseconds.

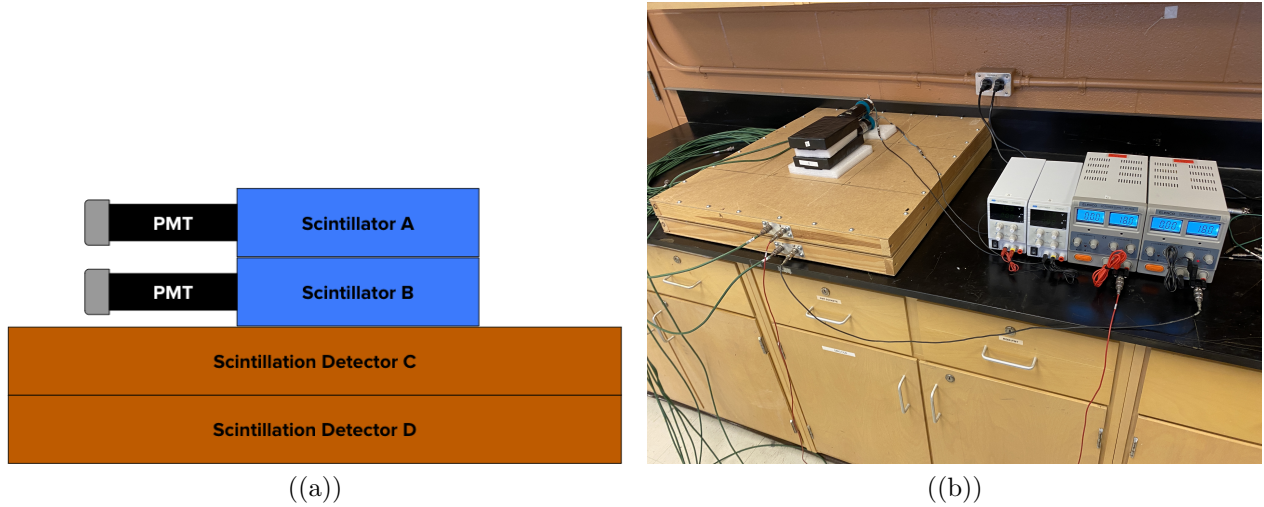


Figure 2: Setup of muon detectors A, B, C, and D used to calibrate the responses. a) Diagram of the apparatus. b) Image of the apparatus in the lab.

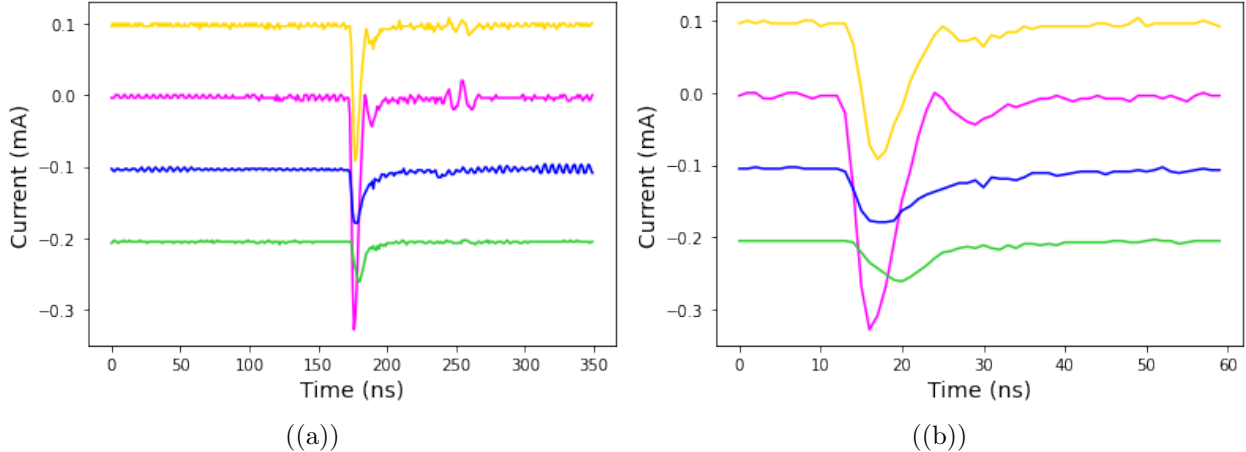


Figure 3: Sample traces for setup used to calibrate scintillator C and D at 18V. a) Total area recorded from oscilloscope. b) Close-up of integrated area that was included into the distribution of charges.

Finally, Moyal curves were graphed over these distributions, and the mean values of the curve fits were extracted as seen in Figure 4. These mean values were graphed, and a parabola was fitted to the data points. The resulting parabola fit was then used to obtain the high voltage values associated with a mean charge of 0.9 pC (see Appendix A for parabola fits). This process was repeated for every detector used in this experiment, with the final voltages

being 19.0 ± 0.03 V for detector C and 19.6 ± 0.02 V for detector D.

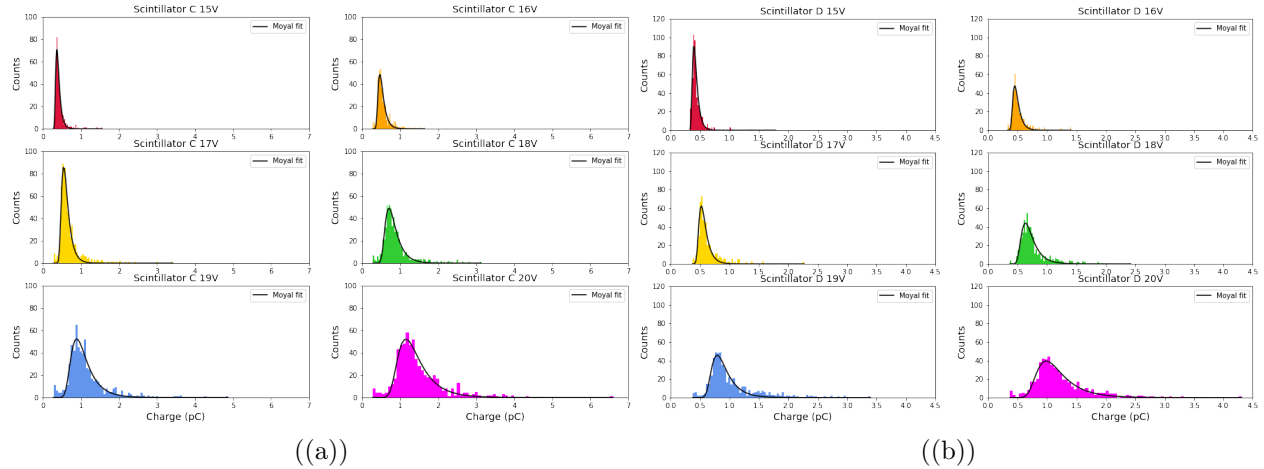


Figure 4: Landau distributions of charges in pC for voltages of 15V, 16V, 17V, 18V, 19V, and 20V, along with Moyal fit. a). Distribution of charges for scintillator C with sample of size $n = 1000$ for all graphs. b). Distribution of charges for scintillator D with sample of size $n = 1000$ for all graphs.

This calibration process was necessary to equalize each detector's response. If the voltage applied to the PMTs were too low, the apparatus would not be fully efficient [12]. On the other hand, applying excessive voltage would stress the PMTs unnecessarily. Moyal curves were used to describe the distribution of the charges as Moyal curves are effective approximations of Landau distributions [13]. More particularly, Landau distributions are probability density functions that describe the distributions of energy loss of a charged particle passing through a medium [12]. Therefore, Landau distributions, along with the Moyal curve approximations, can describe the distribution of charges of incoming muons passing through the scintillation detectors. The equation for a Moyal curve, $g_z(x)$, is expressed as:

$$g_z(x) = \frac{1}{\sqrt{2\pi}\sigma} e^{-\frac{1}{2}[\frac{x-\mu}{\sigma} + e^{-\frac{x-\mu}{\sigma}}]}, \quad (5)$$

where μ is the location parameter and σ is the scale parameter for a random value x in the probability distribution.

2.2 Detector Efficiency

The efficiency of the scintillation detectors C and D was tested by counting instances where detectors A, B, and C would detect a signal and instances where detectors A, B, and D would detect a signal over different voltages (15 V, 16, V, 17 V, 18 V, 19 V, and 20 V) using the setup of Figure 2. The logic behind this process was to use $A \cdot B$ to define the passage of a muon such that $A \cdot B \cdot C$ would be a count for detector C, and $A \cdot B \cdot D$ would be a count for detector D.

This was performed by a NIM discriminator that sent muon pulses to a logic unit that would set off two different counters for an hour, one counter would only consider instances where detectors A, B, and C detected a signal, and the other would only consider instances where detectors A, B, and D detected a signal. Using the assumption that $A \cdot B$ would be identical for the recorded instances of $A \cdot B \cdot C$ and $A \cdot B \cdot D$, as these were measured during the same period, the counts recorded for each detector were plotted with respect to time, shown in Figure 5. Hence, the efficiency of detectors C and D was measured, and the detectors were set to voltages between 18 V to 20 V found within the plateaus observed in Figure 5.

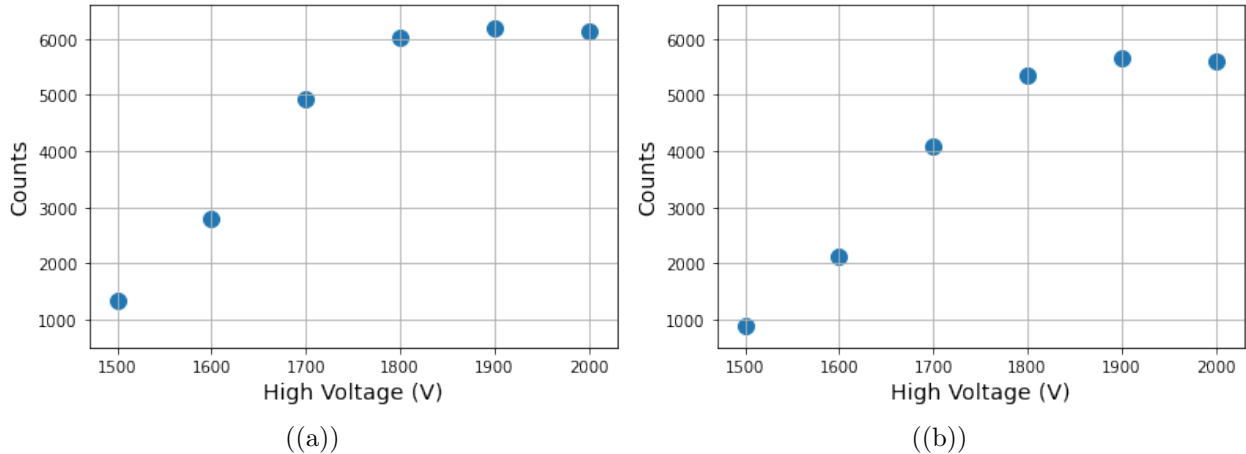


Figure 5: Responses of detectors C and D with relation to tested high-voltages. a) Response of detector C. b) Response of detector D.

2.3 Experimental Design

The experimental design used to measure the decoherence curve of cosmic-ray muons featured the use of two scintillation detectors, C and D, along with an arrangement of NIM modules, specifically a discriminator, logic unit, and counter. In more detail, the data for the muon decoherence curve was collected by measuring instances where detectors C and D received coincident cosmic-ray muons over a period of time at different separations. A total of nine separations were tested, ranging from 0.65 m to 6 m with increments of 0.65 m, which is the length of the detectors. These separations were measured using a laser distance measurer.

The muon coincidences were recorded by sending the detectors' signals through the discriminator, which sent corresponding C and D pulses to the logic unit. The logic unit was set to send out a pulse for instances of muon coincidence, $C \cdot D$, to the counter, which was preset to record pulses over a given period of time. Figure 6 represents the apparatus used for this experiment. Furthermore, the muon coincidences were visualized using a SDS1204X-E SIGLENT oscilloscope connected to a laptop running a Python program.

Thereafter, the decoherence curve was obtained by taking rates of muon coincidences with respect to the distance of the detector separations. The analysis was performed using a Python program using the Numpy and Matplotlib modules.

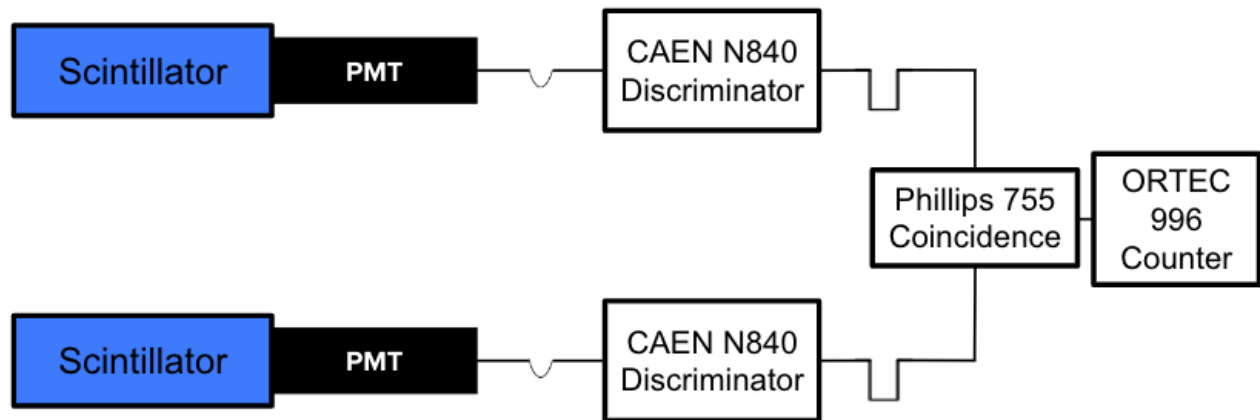


Figure 6: Diagram of apparatus illustrating the logic used to count coincident signals in detectors C and D.

2.4 Time Difference Between Coincident Muons

To verify that the data taken by the apparatus were not affected by bursts or other anomalies, the time differences between muon coincidences for a detector separation of 8.9 m were recorded for a period of 61 hours and 40 minutes using a SDS1204X-E SIGLENT oscilloscope connected to a laptop running a Python program. The distribution of time differences was then graphed, and an exponential fit was applied to the data. This analysis was necessary to demonstrate that the experiment effectively measured muon coincidences as the coincidences are distributed in time according to Poisson statistics.

3 Results

Data collection for muon coincidences was performed for six days using a series of NIM modules to gather the coincidence rates, as shown in Figure 6, and a SDS1204X-E SIGLENT oscilloscope to visualize the data. Each data file used for this experiment contained no more than 3000 traces to ensure that the Python program did not face memory issues when performing the data analysis.

The muon coincidences for a total of six detector separations were recorded. The distribution of the measured coincidence rates for these separations is depicted in Figure 7 with a logarithmic vertical axis, along with an NKG fit created using the Curve Fit module imported from the SciPy Python library. Furthermore, a total of 1747 time differences between traces were measured for a counter separation of 8.9 m for 61 hours and 40 minutes, and the distribution for these data is shown in 8 with a logarithmic vertical axis and an exponential fit performed using Curve Fit.

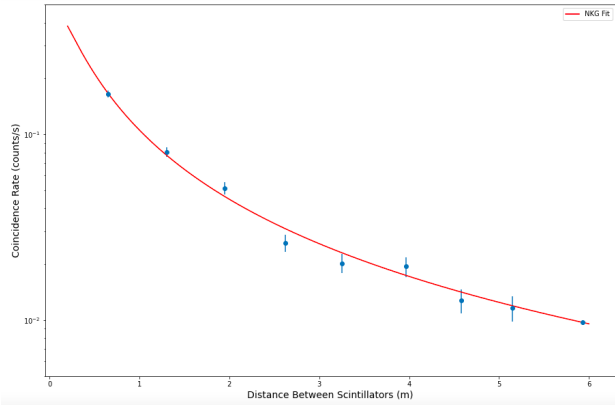


Figure 7: Distribution of coincidence rate in counts per seconds along with NKG fit.

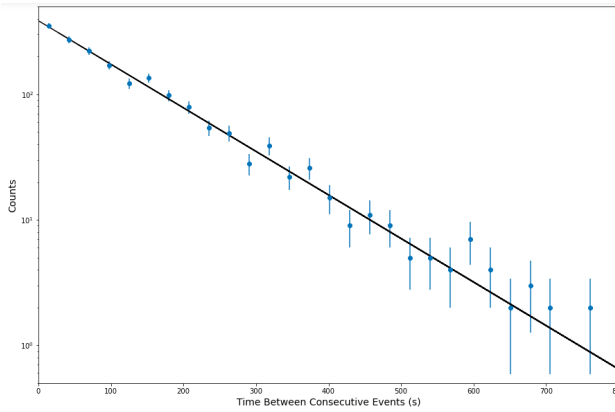


Figure 8: Distribution of time differences between coincidence counts along with exponential fit created through curve fitting and represented by a logarithmic vertical axis, mean time difference of 125.1 ± 2.6 seconds and initial count of 385.7 ± 5.7 .

4 Discussion

The cosmic-ray muon decoherence curve measured in this study is depicted in Figure 7. By characterizing the decoherence curve, this result obtained the following parameters for the NKG fit: an age parameter of $s = 0.92 \pm 0.14$, a Molière radius of $r_m = 37.8 \pm 27$ meters, and a normalization constant of $c(s) = 0.0022 \pm 0.002$. Taking note that the coincidence rates decrease less and less as the detectors' separation increases, it is possible to affirm that the decoherence curve depicted above matches well with the NKG fit.

This is further highlighted by a qualitative analysis of Figure 8, given that the exponential decay pattern exhibited by the distribution of time differences between muon coincidences demonstrates that the experimental design used for this study was not significantly affected

by background noise. This pattern is expected as the timing of the coincidences is assumed to be random but at a constant rate. Therefore, the time differences follow Poisson statistics, and the probability to wait longer between events declines exponentially with waiting time.

Moreover, it must be noted that some limitations affected the data collection as the detectors could only be separated to a distance of 6 m; further separations were limited due to obstructions and the room size.

5 Conclusion

In sum, it is possible to conclude that the experimental setup successfully measured the decoherence curve for cosmic-ray muons. By accurately measuring muon coincidence rates, this study shows excellent capacity in confirming the existence of air showers and characterizing their lateral size using the NKG function. Furthermore, this study demonstrates the Poisson nature of arrival times based on the exponential pattern of time differences. Future studies should consider improving the methods presented here by measuring coincidence rates for extended periods to increase the experimental accuracy of NKG parameters.

6 Acknowledgments

The author of this report would like to thank Prof. David Hanna and Dr. Stephan O'Brien for providing the necessary supervision, feedback, and infrastructure on all the steps of the project.

References

- [1] C. D. Anderson, & S. H. Neddermeyer, "Cloud Chamber Observations of Cosmic Rays at 4300 Meters Elevation and Near Sea-Level," *Physical Review*, vol. 50, no. 4, pp. 263–271, 1936. [Accessed May 27 2022] [1](#)
- [2] D. Lal, & B. Peters, *Cosmic Ray Produced Radioactivity on the Earth*. Berlin & Heidelberg, Germany: Springer, 1967. [Accessed May 30 2022] [1](#)
- [3] R.L. Workman, et al. (Particle Data Group), to be published (2022) [Accessed May 27 2022] [1](#)
- [4] S. Mollerach, & E. Roulet, "Progress in high-energy cosmic ray physics," *Progress in Particle and Nuclear Physics*, vol. 98, pp. 85–118, 2018. [Accessed July 7 2022] [1](#)
- [5] B. Rossi, *High-Energy Particles*. New York, United States of America: Prentice-Hall, 1952. [Accessed May 27 2022] [1](#)
- [6] J. D. Walecka, "Semi-leptonic weak and electromagnetic interactions with nuclei: Muon capture to discrete nuclear levels from hyperfine states," *Nuclear Physics A*, vol. 258, no. 3, pp. 397–416, 1976. [Accessed June 17 2022] [1](#)
- [7] A. Knecht, A. Skawran, & S. M. Vogiatzi, "Study of nuclear properties with muonic atoms," *The European Physical Journal Plus*, vol. 135, no. 10, 2020. [Accessed June 17 2022] [1](#)
- [8] A. Tapia, et al. "The lateral shower age parameter as an estimator of chemical composition," *33ND International Cosmic Ray Conference*, 2013. [Accessed July 7 2022] [2](#)
- [9] K. Kamata, & J. Nishimura, "The Lateral and the Angular Structure Functions of Electron Showers," *Progress of Theoretical Physics Supplement*, vol. 6, pp. 93–155, 1958. [Accessed July 7 2022] [2](#)
- [10] K. Greisen, "Cosmic Ray Showers," *Annual Review of Nuclear Science*, vol. 10, no. 1, pp. 63–108, 1960. [Accessed July 7 2022] [2](#)

- [11] W. R. Leo , *Techniques for Nuclear and Particle Physics Experiments*. Berlin & Heidelberg, Germany: Springer, 1994. [Accessed June 3 2022] [2](#)
- [12] L. Landau, "On the energy loss of fast particles by ionization," *Journal of Physics*, vol. 8, no. 4, pp. 201-205, 1944. [Accessed June 3 2022] [5](#)
- [13] J. E. Moyal, "Theory of ionization fluctuations," *The London, Edinburgh, and Dublin Philosophical Magazine and Journal of Science*, vol. 46, no. 374, pp. 263–280, 1955. [Accessed June 4 2022] [5](#)

A Plotted Means for Detector Calibration

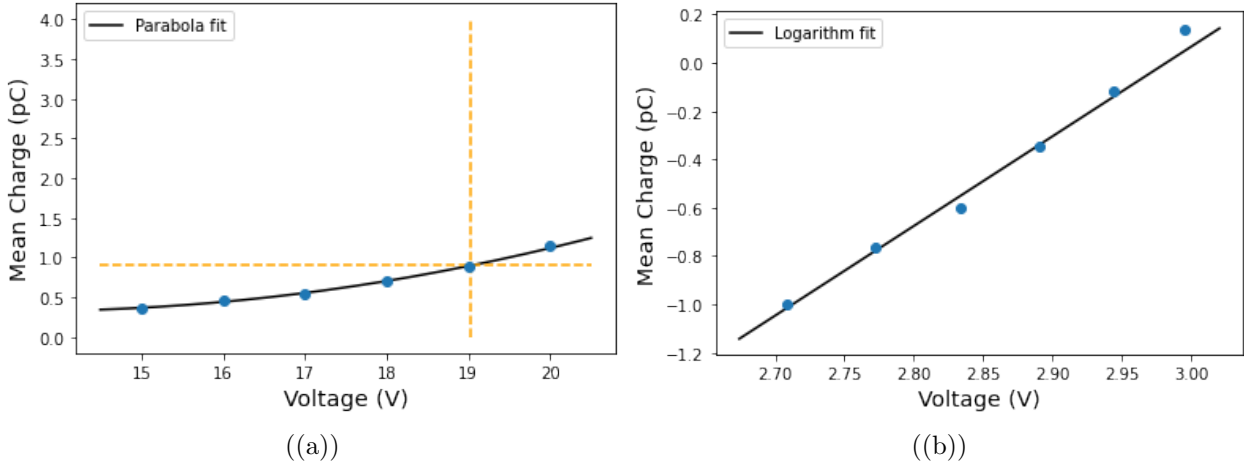


Figure 9: Plotted mean charges for scintillator C used for high-voltage calibration. a) Plotted means with a parabola fit, orange cross centered at point in the parabola that yields a mean charge of 0.9 pC. b) Plotted means with logarithmic scaling and appropriate linear fit.

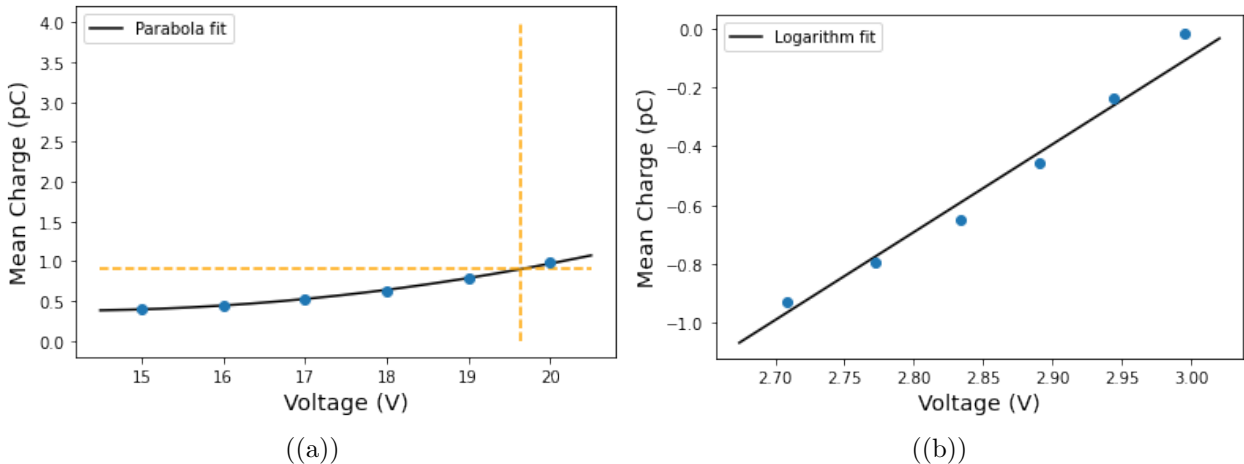
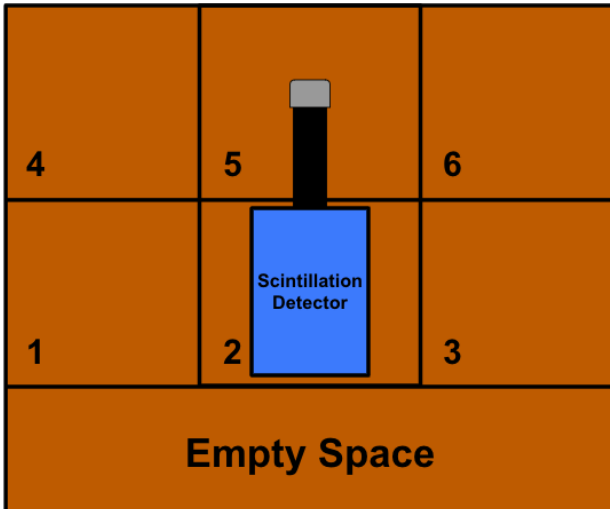


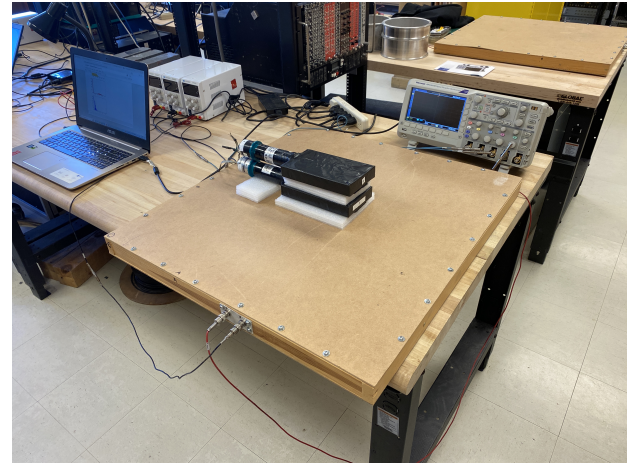
Figure 10: Plotted mean charges for scintillator D used for high-voltage calibration. a) Plotted means with a parabola fit, orange cross centered at point in the parabola that yields a mean charge of 0.9 pC. b) Plotted means with logarithmic scaling and appropriate linear fit.

B Detector Sensitivity

The uniformity of scintillation detectors C and D was evaluated by using detectors A and B as triggers and measuring incoming muon traces in six equal areas ($26.2\text{ cm} \times 21.7\text{ cm}$), as shown in Figure 11. In more detail, the responses on detectors C and D were equalized using the distribution of means obtained during calibration, then detectors A and B were placed in each of the six positions and traces due to through-going muons were recorded. Thereafter, the recorded traces were integrated to obtain the distribution of charges at each of the six positions; these distributions are shown in Figure 12.



((a))



((b))

Figure 11: Experimental setup used to test the sensitivity of muon detectors C and D at multiple points and outline of the tested positions, labeled from 1-6. a) Diagram of the apparatus. b) Image of the apparatus in the lab.

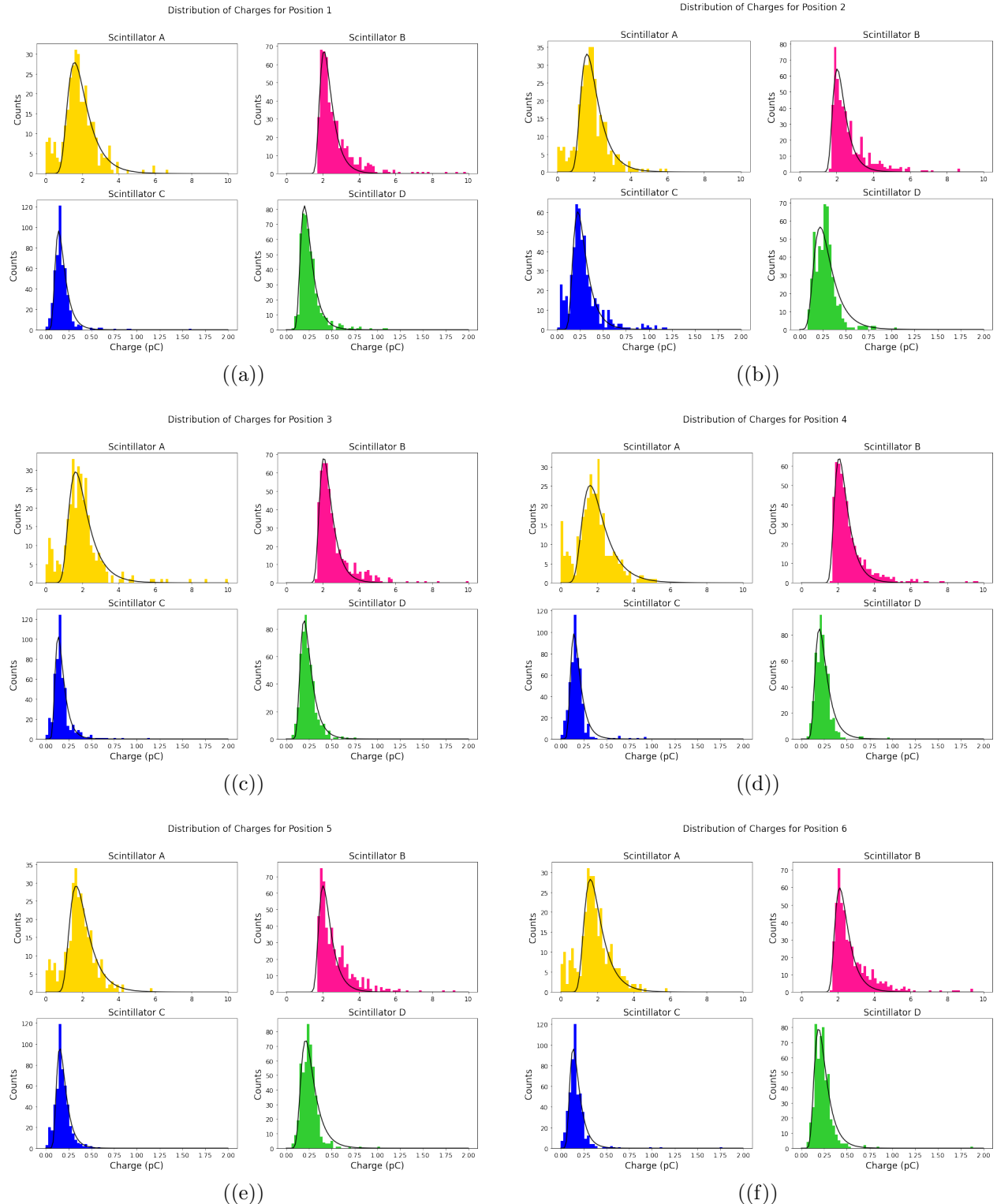


Figure 12: Landau distributions of charges in pC for tested positions 1-6 on detectors C and D with sample of size $n = 500$ for all graphs. a). Distribution of charges for position 1. b). Distribution of charges for position 2. c). Distribution of charges for position 3. d). Distribution of charges for position 4. e). Distribution of charges for position 5. f). Distribution of charges for position 6.